Physically Inspired Circuit Model for Systematic Analysis of Resonant Ion Sensor

Omar ElSherbiny*, Subhanwit Roy*, Sadaf Charkhabi†, Adam Carr†, Andee Beierle†, Nigel Reuel†, Nathan Neihart*‡

* Department of Electrical and Computer Engineering, Iowa State University, Ames, IA, USA

† Department of Chemical and Biological Engineering, Iowa State University, Ames, IA, USA

‡ Corresponding author. Email: neihart@iastate.edu

***Abstract*—Ions play a significant role in biological, industrial, and agricultural processes. Noninvasive, real-time detection of their presence and concentration has become of vital importance in a multitude of processes. In this paper, we present a lumped-element circuit model for an Archimedean spiral inductor based resonant sensor which accurately detects and quantifies ionic concentration of aqueous solutions. The development of the model is guided by observed physical phenomena caused by changing a solution's ionic concentration. The system's response to different concentrations of aqueous potassium chloride is measured, and the model parameters are extracted from measured data. The model parameters are extrapolated to obtain expressions that model the system's response over a wide range of concentrations. There is good agreement between the model and measured data, making it valid for concentrations ranging from 1.66 mmol/L to 1 mol/L. The model helps generate insight into the behavior of the physical system, could be used to systematically optimize the sensor design, and could be extended to other analytes.**

Keywords—dielectric metrology, ion monitoring, lumped element modeling, noninvasive, resonant sensor

I. Introduction

The ubiquity of ions in a plethora of natural processes have interested researchers in their detection for several decades [1]–[3]. However, the need to monitor ions in real-time has burgeoned in modern times, owing to applications such as soil [4] and water treatment [5], tissue monitoring [6], and consumer wearables [7]. To cater to this growing need, resonant dielectric measurement techniques, which observe the change in resonant frequency of a sensor, have been at the forefront of the design of noninvasive, real-time ion sensing systems [8]–[14]. Such sensors are typically designed using empirical, Edisonian experiments, or finite element method (FEM) solvers [12], [15], [16]. While both approaches eventually converge to a practical design, they are time consuming and offer limited insights into the functionality of the sensor. This is particularly problematic when it comes to explaining some of the seemingly obscure behavior patterns of the senor. This problem is mitigated using an equivalent lumped-element circuit model, which often provides a simple, intuitive, resource-efficient approach to investigate the theoretical underpinnings of such a system. Lumped-element circuit modeling, which aims to express complex electromagnetic phenomena in terms of simple circuit theory, has been used extensively to study the electrical behavior of a multitude of physical structures [17]–[20].

In this paper, we investigate an open-circuit Archimedean spiral inductor based resonant sensor geometry which has been previously studied by researchers for measuring different kinds of analytes [13], [14], [21], [22]. A sketch of the system we examine is shown in Fig. 1. The system is comprised of an open-circuit, Archimedean spiral inductor of 20 turns, with a 40 mm outer diameter and a pitch of 1 mm. The inductor is made of copper on a flexible, polyimide substrate which is interrogated by a coplanar, two-loop antenna (reader) which is connected to a vector network analyzer (VNA). The reader antennas are made of 18 AWG wire, each having a diameter of 56 mm, and are separated from the inductor by a 1.7 mm thick Acrylonitrile Butadiene Styrene (ABS) sheet. The inductor is adhered to the base of a petri dish which hosts the sample under test, and the petri dish is positioned on the ABS sheet. The mechanism of transduction is the change in resonant frequency of the inductor when the concentration of the analyte is varied. The noncontact geometry allows the sensor to avoid corrosion and electrode polarization [23],

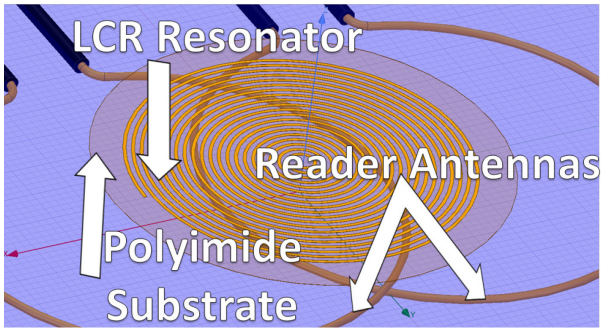

Fig. 1. Closeup sketch of the open-circuit Archimedean spiral inductor based resonant sensor showing the spiral inductor coil, polyimide substrate, and two-loop reader antennas.

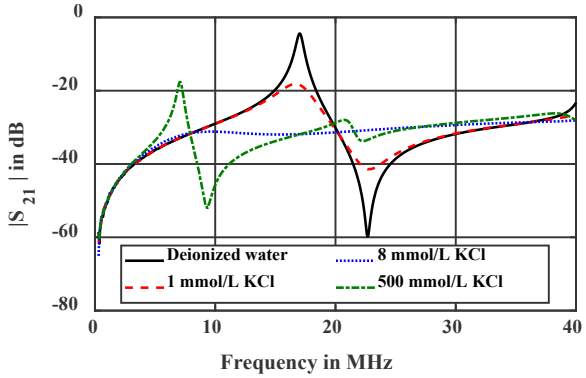

Fig. 2. Measured transmission spectra of the Archimedean spiral inductor based resonant sensor at different concentrations of KCl. The transmission peaks at 17 MHz, 16.67 MHz, and 7.1 MHz, which correspond to the resonant frequencies at 0 mmol/L (deionized water), 1 mmol/L, and 500 mmol/L of aqueous KCl, respectively. The resonant behavior disappears for a KCl concentration on 8 mmol/L

TABLE I. CONCENTRATION, RELATIVE PERMITTIVITY , AND AVERAGE EFFECTIVE CONDUCTIVITY FOR AQUEOUS SOLUTIONS OF KCL AT 25 ˚C [24]

c (mmol/L)	ε_{soln}	σ_{soln} (S/m)	c (mmol/L)	ε_{soln}	σ_{soln} (S/m)
3	78.43	0.048	60	77.88	0.783
8	78.38	0.119	500	73.78	5.681
15	78.31	0.214	1000	69.38	10.857

making it conducive to a host of agricultural and healthcare processes.

In this paper, we specifically investigate the performance of the sensor under varying concentrations of aqueous potassium chloride (KCl). Measurement results show a shift in resonant frequency, identified by a peak in $|S_{21}|$, with concentration, shown in Fig. 2. We observe that increasing the ionic concentration leads to a decrease in resonant frequency. This is seemingly peculiar as Table I, which is adapted from [24], shows that the relative permittivity, ε_{soln}, of aqueous KCl decreases with increasing concentration, and one readily expects resonant frequency to increase with decreasing ε_{soln}. Furthermore, it is seen in Fig. 2 that the resonant behavior disappears for concentrations near 8 mmol/L, but is present for both higher and lower concentrations. This observation calls for a detailed understanding of the sensor behavior.

Hence, to facilitate the analysis, we developed a lumped-element circuit model of the sensing system that is valid from a concentration of 1.66 mmol/L to 1 mol/L, and captures the trends observed in empirical testing. Each parameter of the model is included to represent some physical aspect of the real system, and this allows us to build an intuition for the observed trend in shift of resonant frequency with change in sample concentration. It further provides insight into the transfer of power between the inductor and the solution, which helps us address the question of disappearance and reappearance of resonance with changing ionic concentration, as seen in Fig. 2. Finally, the developed model opens doors to systematic

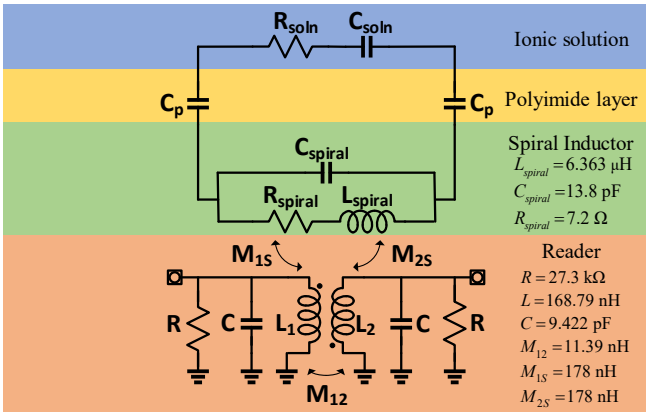

Fig. 3. Proposed physically inspired lumped-element circuit model of the resonant sensing system showing separate parts for the reader, resonator, polyimide layer, and ionic solution.

optimization of the sensing system, which is not possible through empirical testing or FEM simulations.

II. LUMPED-ELEMENT CIRCUIT MODEL EXTRACTION

A. Lumped-Element Components

The proposed lumped-element circuit model of the resonant sensor-reader system is illustrated in Fig. 3. Each component in the model represents a physical aspect of the real system.

The spiral inductor is modeled as an inductor in series with a resistor to account for its resistive losses. Additionally, a capacitor is added in parallel to realize the interwinding capacitance of the inductor. The self-inductance was approximated using [25]:

$$L_{spiral} = \frac{1}{2}\mu_0 N^2 d_{avg}\left(\ln\left(\frac{2.46}{\rho}\right)+0.2\rho^2\right) \quad (1)$$

where μ_0 is the permeability of free space, N is the number of turns in the spiral, d_{avg} is the average diameter of the inductor, and ρ is its fill factor. The self-resonant frequency is approximated using [26]:

$$f_{sr} = \frac{c}{2l\sqrt{\varepsilon_r}}\left(0.182(N)^{-0.46}+0.72\right) \quad (2)$$

Where l is the total length of the spiral inductor, and ε_r is the relative permittivity of the deionized (DI) water. The resistance is calculated to account for the skin effect using:

$$R_{spiral} = \frac{l}{2r}\sqrt{\frac{\mu_0 f_{sr}}{\pi\sigma}} \quad (3)$$

where r is the cross-sectional radius of the conductor, σ is the conductivity of copper. The capacitance is calculated from the self-resonant frequency using:

$$C_{spiral} = \frac{1}{(2\pi f_{sr})^2 L_{res}} \quad (4)$$

To model the aqueous KCl solution, we look into its dielectric properties, which are stated in terms of its relative permittivity, ε_{soln}, and conductivity, σ_{soln}. The relative

permittivity represents the sample polarization, whereas conductivity denotes the loss in the system due to the presence of ions. Increasing the concentration of ions in the solution changes both its relative permittivity and conductivity : a phenomenon which has been thoroughly studied in literature [24]. Specifically, the relative permittivity decreases and the conductivity increases, as shown in Table I. To model this behavior, we use a series *RC*-circuit, where we expect C_{soln} and R_{soln} to decrease with increasing concentration. Moreover, the presence of the polyimide substrate affects the polarization between the inductor and the solution, which in turn, increases the parasitic capacitance between the spiral inductor and the solution. The capacitance of the polyimide substrate is modeled as C_p and its value is approximately proportional to the area occupied by the inductor, and can be estimated by:

$$C_p = 4\pi r^2 \frac{\varepsilon_0 \varepsilon_p}{t_p} \tag{5}$$

where r is the cross-sectional radius of the conductor, ε_p and t_p are the relative permittivity and thickness of the polyimide substrate, respectively, and ε_0 is the permittivity of free space. However, by definition, a capacitor is comprised of two conductors carrying equal but opposite charges. In this case, one 'conductor' of the capacitor is formed by the aqueous solution and its conductivity depends on the ionic concentration of the solution. Therefore, it is expected that C_p will be dependent on the ionic concentration, and that (5) is only valid when the concentration of the solution is high.

Finally, the two-loop reader is represented by a pair of coupled *RLC*-resonators. Two mutual inductance parameters, M_{1S} and M_{2S} are used to denote the magnetic coupling between the two loops of the reader and the spiral inductor.

B. *Extraction of Component Values*

The spiral inductor was exposed to 40 different concentrations of KCl, ranging from 0 mol/L (DI water) to 1 mol/L. The sensor's two-port S-parameter response was recorded from 300 kHz to 100 MHz using an Agilent E5071C 4-port VNA, calibrated such that the reference plane was at the terminals of the reader. Component values for the coupled *RLC*-resonators, modeling the reader, were extracted using Keysight Advanced Design System (ADS) from measured S-parameters when the analyte is DI water. Additionally, initial parameters for L_{spiral}, R_{spiral}, and C_{spiral} are calculated using (1)-(4), then the final parameters are fine-tuned in ADS based on measured S-parameters. The component values for the reader and spiral inductor are invariant with analyte concentration, and their final values are presented in Fig. 3.

The dependence of the resistance and capacitance of the ionic solution on ionic concentration, has been rigorously studied in [27]; however, the study was based on electrochemical impedance spectroscopy which necessitates the use of electrodes to make galvanic contact to the liquid that is to be measured. Conversely, C_{soln} and R_{soln} in Fig. 3 arise due to an electromagnetically induced emf in the ionic solution: a phenomenon which, to date, has not been well modeled using closed-form expressions. In this regard, closed-form expressions, to calculate the concentration-dependent component values, were generated by curve fitting the simulated S-parameters at six different concentrations of KCl. This curve fitting was guided by the physical phenomena of decreasing relative permittivity and increasing conductivity, with increasing concentration, presented in Table I. The expressions are given in (6)-(8) as:

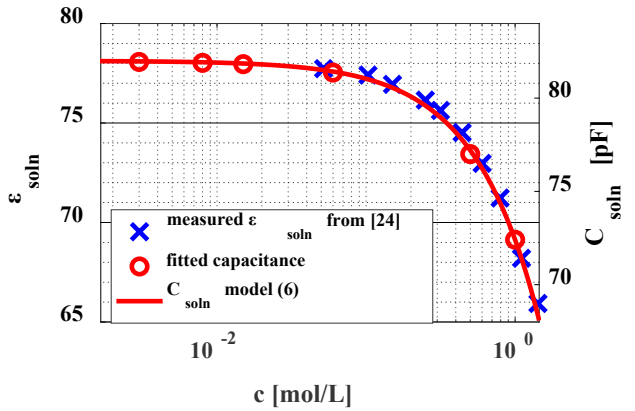

Fig. 4. Plot of relative permittivity, ε_{soln}, and modeled solution capacitance, C_{soln}, versus concentration of aqueous KCl solution showing that decrease in solution capacitance follows a decrease in sample permittivity. The fitted linear relationship between solution capacitance and sample concentration is also provided.

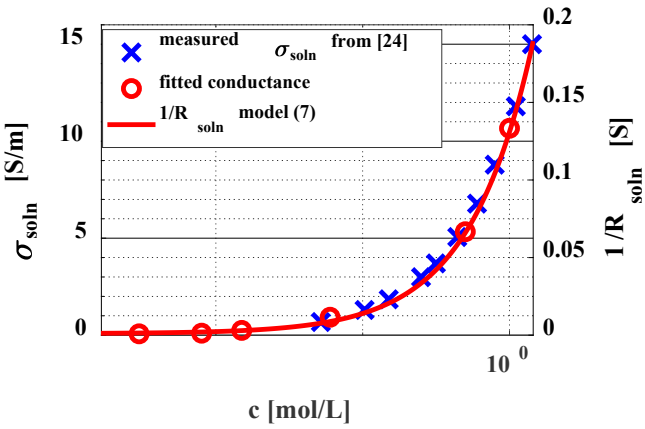

Fig. 5. Plot of solution conductivity, σ_{soln}, and modeled solution conductance, $1/R_{soln}$, versus concentration of aqueous KCl solution showing that increase in solution conductance follows an increase in sample conductivity. The fitted rectangular hyperbolic relationship between solution resistance and sample concentration is also provided.

$$C_{soln} = 82 - 9.6c \tag{6}$$

$$\frac{1}{R_{soln}} = 0.13c + 0.001 \tag{7}$$

$$C_p = 200\ln(c) + 1280 \tag{8}$$

where c is the concentration of KCl in mol/L, and C_p and C_{soln} are in pF.

Figs. 4-6 illustrate the dependency of C_{soln}, R_{soln} and C_p on the solution's concentration. Fig. 4 and Fig. 5 show the measured relative permittivity and conductivity from [24]. It can be seen that the modeled values for $1/R_{soln}$ and C_{soln} show

the same dependence on concentration as the conductivity, σ_{soln}, and relative permittivity, ε_{soln}. Furthermore, at a high concentration of KCl, C_p approaches the value predicted by (4). At a concentration of 1450 mmol/L, the extrapolated capacitance is 1.354 nF, and the value predicted by (4) is 1.338 nF, a difference of 1.2%.

III. Model Validation and Discussion

Given (6)-(8), we can use the lumped element model in Fig. 3 to predict the behavior of the physical system. To demonstrate the validity of our model, the magnitude and phase of the simulated transmission spectra for concentrations of 4.99 mmol/L, 21.77 mmol/L, and 100 mmol/L are plotted in Fig. 7. These concentrations values are different that what was used to generate the model and it is seen that there is good agreement between the model and the measured data.

The model provides insight into the disappearance of the resonance around a concentration of 8 mmol/L and its subsequent reemergence. The model's open-circuited resonant system, discounting the reader, can be analyzed as a matching network between the spiral inductor coil impedance and the solution impedance. At concentrations when there is a large mismatch between the two impedances, reflections allow very little power to be transferred from the coil to the sample medium, thus inhibiting the transfer of energy via the solution. This manifests in the suppression of the peaking of the overall $|S_{21}|$. This observation opens doors to further optimization of the inductor coil to get a better match between the coil impedance and solution impedance at concentrations of interest, and thus get sharper resonant peaks.

IV. Conclusion

This paper presented a lumped-element circuit model of an Archimedean spiral inductor based resonant sensor for measuring ionic concentration in aqueous KCl solutions. The model has been motivated by physical aspects of the sensing system as well as the analyte environment, and is extracted using measured response of the sensor for six different ionic concentrations. The model can successfully predict the sensor response over a wide range of KCl concentrations (1.66 mmol/L to 1 mol/L). Moreover, the model parameters are shown to follow simple, physically intuitive relationships with concentration, making the model more insightful than experiments and FEM simulations. The insights generated from the model help provide explanations for the trend in resonant frequency with changing ionic concentration, and the disappearance of resonance at a critical concentration and its subsequent reemergence. In the future, the model could be used to study the sensor response to other types of analytes, as well as to develop an approach to systematically optimize the sensing system.

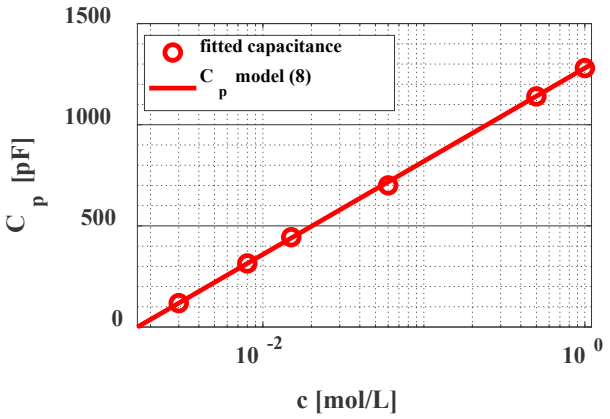

Fig. 6. Plot of polyimide layer capacitance C_p versus concentration of aqueous KCl solution. The fitted logarithmic relationship between polyimide layer capacitance and sample concentration is also provided.

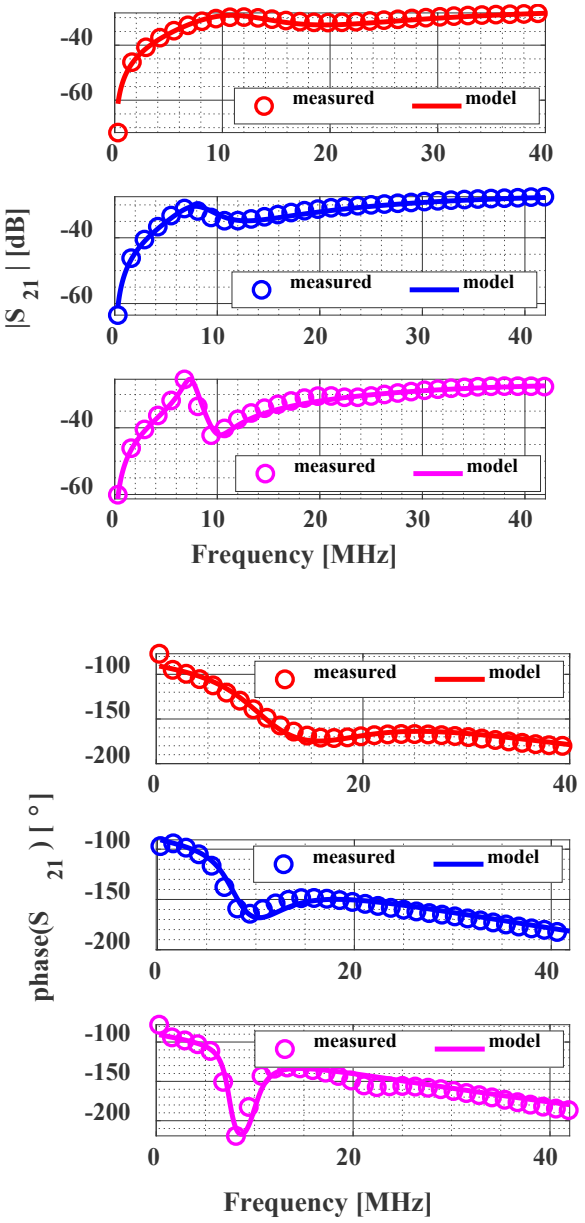

Fig. 7. (a) Magnitude and (b) phase of transmission spectra obtained using the lumped element circuit model, showing good agreement with measured data, thus confirming the validity of the developed model.

REFERENCES

[1] P. J. Milham, A. S. Awad, R. E. Paull, and J. H. Bull, "Analysis of plants, soils and waters for nitrate by using an ion-selective electrode," *Analyst*, vol. 95, no. 1133, pp. 751–757, 1970.

[2] U. Kaatze and Y. Feldman, "Broadband dielectric spectrometry of liquids and biosystems," *Meas. Sci. Technol.*, vol. 17, no. 2, pp. R17–R35, Dec. 2005.

[3] A. Gorji, A. Kaleita, and N. Bowler, "Towards low-cost sensors for real-time monitoring of contaminant ions in water sources," in *2017 IEEE MTT-S International Microwave Symposium (IMS)*, 2017, pp. 529–532.

[4] N. Harris, A. Cranny, M. Rivers, K. Smettem, and E. G. Barrett-Lennard, "Application of Distributed Wireless Chloride Sensors to Environmental Monitoring: Initial Results," *IEEE Trans. Instrum. Meas.*, vol. 65, no. 4, pp. 736–743, Apr. 2016.

[5] O. Korostynska, A. Mason, and A. I. Al-Shamma'a, "Monitoring Pollutants in Wastewater: Traditional Lab Based versus Modern Real-Time Approaches," in *Smart Sensors for Real-Time Water Quality Monitoring*, S. C. Mukhopadhyay and A. Mason, Eds. Berlin, Heidelberg: Springer, 2013, pp. 1–24.

[6] M. F. Farooqui and A. Shamim, "Low Cost Inkjet Printed Smart Bandage for Wireless Monitoring of Chronic Wounds," *Sci. Rep.*, vol. 6, p. 28949, Jun. 2016.

[7] M. Bariya, H. Y. Y. Nyein, and A. Javey, "Wearable sweat sensors," *Nat. Electron.*, vol. 1, no. 3, pp. 160–171, Mar. 2018.

[8] A. P. Gregory and R. N. Clarke, "A review of RF and microwave techniques for dielectric measurements on polar liquids," *IEEE Trans. Dielectr. Electr. Insul.*, vol. 13, no. 4, pp. 727–743, Aug. 2006.

[9] G. S. P. Castle and J. Roberts, "A microwave instrument for the continuous monitoring of the water content of crude oil," *Proc. IEEE*, vol. 62, no. 1, pp. 103–108, Jan. 1974.

[10] J. Roberts and F. Wang, "Dielectric Relaxation in Water Over the Frequency Range 13≤f≤18 GHz Using a Resonantmicrowave Cavity Operating in the TM010 MODE," *J. Microw. Power Electromagn. Energy*, vol. 28, no. 4, pp. 196–205, Jan. 1993.

[11] J. Krupka, K. Derzakowski, and J. Baker-Jarvis, "TE018 Dielectric-Resonator Technique for Precise Measurements of the Complex Permittivity of Lossy Liquids at Frequencies Below 1 GHz*," 2004, pp. 469–470.

[12] S. Roy, N. M. Neihart, and N. Bowler, "Coaxial microwave resonant sensor design for monitoring ionic concentration in aqueous solutions," in *2018 IEEE International Instrumentation and Measurement Technology Conference (I2MTC)*, 2018, pp. 1–6.

[13] K. G. Ong, J. Wang, R. S. Singh, L. G. Bachas, and C. A. Grimes, "Monitoring of bacteria growth using a wireless, remote query resonant-circuit sensor: application to environmental sensing," *Biosens. Bioelectron.*, vol. 16, no. 4, pp. 305–312, Jun. 2001.

[14] M. C. Hofmann, F. Kensy, J. Büchs, W. Mokwa, and U. Schnakenberg, "Transponder-based sensor for monitoring electrical properties of biological cell solutions," *J. Biosci. Bioeng.*, vol. 100, no. 2, pp. 172–177, Aug. 2005.

[15] S. Charkhabi, Y. J. Chan, D.-G. Hwang, S. T. Frey, M. D. Bartlett, and N. F. Reuel, "Kirigami-Enabled, Passive Resonant Sensors for Wireless Deformation Monitoring," *Adv. Mater. Technol.*, vol. 4, no. 5, p. 1800683, 2019.

[16] F.-H. Villa-López, S. Thomas, M. Cole, and J. W. Gardner, "Finite element modelling of particle sensors based on Solidly Mounted Resonators," in *2014 IEEE SENSORS*, 2014, pp. 574–577.

[17] R. W. Cernosek, S. J. Martin, A. R. Hillman, and H. L. Bandey, "Comparison of lumped-element and transmission-line models for thickness-shear-mode quartz resonator sensors," in *Proceedings of International Frequency Control Symposium*, 1997, pp. 96–104.

[18] Y. K. Koutsoyannopoulos and Y. Papananos, "Systematic analysis and modeling of integrated inductors and transformers in RF IC design," *IEEE Trans. Circuits Syst. II Analog Digit. Signal Process.*, vol. 47, no. 8, pp. 699–713, Aug. 2000.

[19] S. C. Rustagi and Chun-Geik Tan, "Equivalent circuit models for stacked spiral inductors in deep submicron CMOS technology," in *2003 IEEE International Symposium on Circuits and Systems (ISCAS)*, 2003, vol. 1, pp. I–I.

[20] C. Bonomo, L. Fortuna, P. Giannone, and S. Graziani, "A circuit to model the electrical behavior of an ionic polymer-metal composite," *IEEE Trans. Circuits Syst. Regul. Pap.*, vol. 53, no. 2, pp. 338–350, Feb. 2006.

[21] S. Charkhabi, "Resonant sensors for passive, real-time, and wireless characterization of biological analytes," *Grad. Theses Diss.*, Jan. 2018.

[22] J. R. Dávila, J. C. P. Gutierrez, and R. P. Blanco, "Use of Magnetic Induction Spectroscopy in the Characterization of the Impedance of the Material with Biological Characteristics," *Adv. Asp. Spectrosc.*, Aug. 2012.

[23] P. B. Ishai, M. S. Talary, A. Caduff, E. Levy, and Y. Feldman, "Electrode polarization in dielectric measurements: a review," *Meas. Sci. Technol.*, vol. 24, no. 10, p. 102001, Aug. 2013.

[24] T. Chen, G. Hefter, and R. Buchner, "Dielectric Spectroscopy of Aqueous Solutions of KCl and CsCl," *J. Phys. Chem. A*, vol. 107, no. 20, pp. 4025–4031, May 2003.

[25] S. S. Mohan, M. del Mar Hershenson, S. P. Boyd, and T. H. Lee, "Simple accurate expressions for planar spiral inductances," *IEEE J. Solid-State Circuits*, vol. 34, no. 10, pp. 1419–1424, Oct. 1999.

[26] J. W. Hooker *et al.*, "An Empirical Expression to Predict the Resonant Frequencies of Archimedean Spirals," *IEEE Trans. Microw. Theory Tech.*, vol. 63, no. 7, pp. 2107–2114, Jul. 2015.

[27] G. Jaffé and J. A. Rider, "Polarization in Electrolytic Solutions. Part II. Measurements," *J. Chem. Phys.*, vol. 20, no. 7, pp. 1077–1087, Jul. 1952.